SGW-33851
Revision 0

Inorganic Plume Delination using Surface High Resolution Electrical Resistivity at the BC Cribs and Trenches Site, Hanford

Prepared for the U.S. Department of Energy
Assistant Secretary for Environmental Management

Project Hanford Management Contractor for the
U.S. Department of Energy under Contract DE-AC06-96RL13200

FLUOR®
P.O. Box 1000
Richland, Washington

SGW-33851
Revision 0

Inorganic Plume Delination using Surface High Resolution Electrical Resistivity at the BC Cribs and Trenches Site, Hanford

J. B. Fink
D. F. Rucker
hydroGEOPHYSICS, Inc.

Date Published
May 2007

U.S. Department of Energy

Published in
Vadose Zone Journal

Prepared for the U.S. Department of Energy
Assistant Secretary for Environmental Management

Project Hanford Management Contractor for the
U.S. Department of Energy under Contract DE-AC06-96RL13200

FLUOR®
P.O. Box 1000
Richland, Washington

J. D. Aardal 05/29/2007
Release Approval Date

Approved for Public Release;
Further Dissemination Unlimited

Inorganic Plume Delineation using Surface High Resolution Electrical Resistivity at the BC Cribs and Trenches Site, Hanford

Abstract

A surface resistivity survey was conducted on the Hanford Site over a waste disposal trench that received a large volume of liquid inorganic waste. The objective of the survey was to map the extent of the plume that resulted from the disposal activities approximately 50 years earlier. The survey included six resistivity transects of at least 200m, where each transect provided two-dimensional profile information of subsurface electrical properties. The results of the survey indicated that a low resistivity plume resides at a depth of approximately 25-44 m below ground surface. The target depth was calibrated with borehole data of pore-water electrical conductivity. Due to the high correlation of the pore-water electrical conductivity to nitrate concentration and the high correlation of measured apparent resistivity to pore-water electrical conductivity, inferences were made that proposed the spatial distribution of the apparent resistivity was due to the distribution of nitrate. Therefore, apparent resistivities were related to nitrate, which was subsequently rendered in three dimensions to show that the nitrate likely did not reach the water table and the bounds of the highest concentrations are directly beneath the collection of waste sites.

Introduction

The Hanford Site, located in eastern Washington, is the center of one of most extensive cleanup operations in the nation (Gephart and Lundgren, 1998). The cleanup effort is the result of past processes dedicated to the production of weapons material during the Cold War. The reprocessing of irradiated uranium produced large quantities of liquid waste that was disposed or stored in a number of ways, including single- and double-shelled underground storage tanks, cribs, trenches, French drains, reverse wells, and ponds. By one estimate, there was approximately $1x10^6$ ML (megaliters) of waste disposed directly to the ground, whereas 200 ML of liquid waste is currently stored in the 177 underground storage tanks (Corbin et al., 2005).

One of the chemical plants, U-Plant, was responsible for the reprocessing of tank waste to extract uranium in a recovery process. The plant operated from 1952-1958 and much of the post-recovery waste was diverted to the BC Cribs and Trenches (BCCT) site, a waste disposal facility south of the 200 East Area in the central portion of the Hanford Site. The waste was generally neutral to basic in pH and contained high amounts of inorganic salts with significant amounts of radionuclides including uranium, plutonium, and fission products (U.S. DOE, 2003). Additionally, the BCCT site received the largest inventory of technetium-99 ever disposed to the ground at Hanford, which equated to approximately 410 Ci (Kincaid et al., 2006).

The design concept behind direct disposal of liquid to the unlined trenches and cribs at BCCT was referred to as specific retention. It was expected that the soil would retain the radiological constituents through ion exchange and prevent much of the waste from reaching the water table. The cribs were funnel-shaped with sloping sides and open bottoms located a few meters below ground surface. The cribs received waste in 42 m^3 (~11,000 gal.) batches from a collection tank through piping that connected the cribs. Most of the crib plumbing is still in place, as verified by electromagnetic and magnetic surveys (Rucker and Sweeney, 2004). Trenches, on the other

hand, were large open ditches approximately 154 meters long, a few meters wide and a few meters deep. An above-ground piping network, most of which was removed (Rucker and Sweeney, 2004) delivered the liquid waste to the trenches.

Since disposal, several borehole geophysical studies were completed at the BCCT site to ascertain the effectiveness of the waste sites to adhere to the provisions of specific retention (Brodeur et al., 1993; Fecht et al., 1977; Horton et al., 2000). The studies were aimed at quantifying the vertical migration of several radiological constituents of the waste including Cesium-137, Cobalt-60, Antimony-125, and Europium-154. The studies showed that no significant vertical migration had occurred for these constituents from 1977 to 1999.

More recently, borehole core samples taken from the center of one of the disposal trenches has confirmed the presence of chlorides, nitrates, sulfates and other salts down to 44 meters below ground surface (Serne and Mann, 2004). Based on the borehole results and modeling, it did not appear that inorganic contamination had reached the water table. Lateral migration of the contaminant plume is postulated as a likely explanation for the limited vertical distribution. For lateral migration to occur, alternating layers of coarse and fine grained (or wet and dry) sediments likely direct the contaminated liquid away from the source zone. Ward et al. (2004) describes the importance of using saturation-dependent anisotropic properties to accurately model flow and transport at the Hanford site.

Owing to the expense of borehole core sampling, a surface geophysical method was employed at the BCCT site to map the subsurface electrical properties to understand the extent to which the waste has migrated. Electrical resistivity was chosen since the high concentration of nitrate in the vadose zone provided a suitable target for mapping. The resistivity method is also capable of imaging deeper than other electromagnetic (EM) methods at sufficient resolution. Paine (2003) presented an airborne EM study of a chloride plume, but the resolution was lower than typical resistivity surveys. For example, Watson et al. (2005) demonstrated that electrical resistivity could map a nitrate plume below the water table down to depths of approximately 20 meters below ground surface using a dipole-dipole array. Adepelumi et al. (2005) and Titov et al. (2005) also used a dipole-dipole array to map shallow plumes beneath waste sites. Benson et al. (1997), Abu-Zeid et al. (2003), and Chambers et al. (2006) used a Wenner array to map the extent of an inorganic and organic (jet fuel) plume down to several meters.

Although the above examples were successful at mapping shallow plumes, the plumes at the BCCT site are much deeper. Therefore, two objectives are outlined for this study: 1) to present a case study of electrical resistivity measurements at a nuclear waste disposal facility and demonstrate that the vadose zone can be mapped in excess of 50 meters below ground surface at sufficient resolution to determine the extent of liquid waste migration, 2) demonstrate that apparent resistivity data from parallel lines can be used to qualitatively assess plume extent and depth in the vadose zone, and 3) that tomographic inversion of electrical resistivity using commercial resistivity inversion codes can give a quantitative assessment of the plume through direct comparison with borehole data. The resistivity mapping is accomplished with modern resistivity equipment and using a less common array type referred to as the pole-pole array. Like the other array types, the pole-pole array requires the use of four poles to complete a single measurement. However, one pole from each of the current source and potential measurement is

placed effectively at infinity. With this arrangement, the pole-pole array configuration provides at least twice as many data measurements as the more common dipole-dipole array and three times that of a Wenner array. Lastly, the mapping technique and correlative methodology could potentially be upscaled to image electrical properties beneath the entire site to understand the large-scale distribution of nitrate beneath each of the trenches and cribs.

Research Site

Within the BCCT (Figure 1), are 20 trenches and 6 cribs over an area of approximately 20 hectares. Of particular interest is Trench 216-B-26, due to the relatively heavy loads of both highly mobile contaminant (nitrate and technetium) and those of low mobility (plutonium, strontium and cesium), as characterized by their respective partition coefficients (Cantrell et al., 2003). The trench was operated from February 1957 to April 1957 and received approximately 5880 m^3 of liquid with $9.45x10^5$ kg of nitrate. The trench also received $4.3x10^5$ kg of sodium, $3.2x10^4$ kg of phosphate, $5.6x10^4$ kg of sulfate, $1.9x10^4$ kg of fluoride, and $1.3x10^4$ kg of chloride (Corbin et al., 2005).

Figure 1. Hanford basemap showing the location of BCCT.

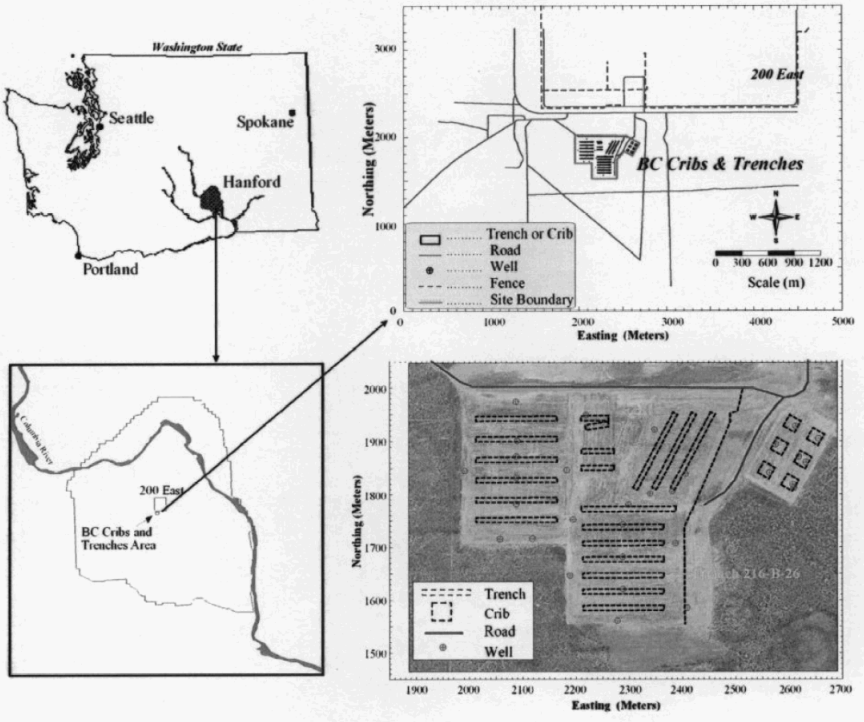

The research site is located within Hanford's central plateau, which has been well characterized due to the high number of contaminated sites. The area is underlain by a thick vadose zone, where the water table is approximately 100m below ground surface. Connelly et al. (1992) describes the hydrostratigraphy of the area as having five main units: 3 units within the Hanford Formation (upper gravel dominated, middle sand dominated, and lower gravel dominated) and 2

units within the Ringold Formation. The Hanford Formation extends down to about 85m below ground surface. The water table is in the upper Ringold Formation, which sits directly on basalt. In 1982, a surficial sandy layer of approximately 0.3m was placed over the entire BCCT site to minimize impacts of radiological releases from local flora and fauna (O'Farrell and Gilbert, 1975).

Figure 2. Borehole data from C4191 showing lithology, water content, nitrate, phosphate, technetium, and pore-water electrical conductivity (adapted from Serne and Mann, 2004).

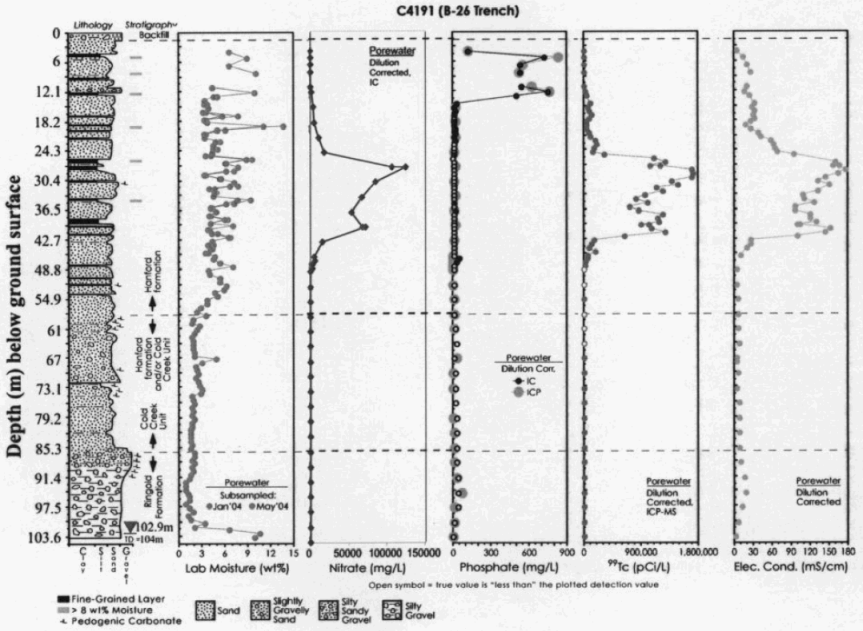

In February 2004, a characterization borehole, labeled C4191, was drilled in the center of Trench 216-B-26. Grab samples of soil (~1 kg of soil) from this borehole were collected every 0.76 meters (2.5 feet) from 5.3 to 104m below ground surface. A total of 124 samples were taken and 39 were characterized for various inorganic and radiological constituents. The soil samples were taken to the Pacific Northwest National Laboratory (PNNL) for sampling analyses, which included moisture content, gamma energy, and water dilution tests to extract pore-water for pH, soil pore water electrical conductivity (EC), and major anions and cations. Moisture content included a thermogravimetric analysis. The soluble inorganic constituents were extracted with a 1:1 dionized-water-to-soil sediment extraction method (Serne et al., 2002). The water extraction method was necessary due to the low volume of antecedent moisture content, which was typically less than 50 mL.

Figure 2 shows the data for a few of these measurements that are pertinent to this study, including lithologic/stratigraphic characterization, water content, electrical conductivity (EC) of the pore-water, and concentrations of nitrate, phosphate, and technetium (Serne and Mann, 2004). The data in Figure 2 show a few important elements that were key to initiating a geophysical electrical resistivity survey over the trench. Firstly, the water content within the Hanford Formation (upper 60m) is generally less than 8% by weight with a variance that mimics the general lithology. Below the Hanford Formation, and continuing to the water table, the water

content decreases to about 3% with the variability also decreasing. The second main observation is that the nitrate and technetium concentrations are very high between 25 and 44m below ground surface (bgs), which correlate well with the extremely high EC in the same depth section. There is a direct causal relationship between the nitrate and EC, where the ionic strength of pore water directly influences the EC. Griffin and Jurinak (1973) suggested that a linear relationship exists between ionic strength and EC from soil extracts, and Marion and Babcock (1976) found a better fit to ionic strength with log-transformed values of EC. A site-specific petrophysical relationship demonstrating the effect of moisture content and electrical resistivity (or conductivity) has yet to be developed for the BCCT.

The technetium concentration does not directly influence the EC. Figure 2 presents the Tc-99 in units of pCi/L, with a maximum around $1.4x10^6$ pCi/L. The conversion for a mass-based concentration of this radionuclide is approximately $1.69x10^7$ pCi/mg, equating to a maximum mass concentration of 0.08 mg/L. The high correlation between EC and Tc-99 is noncausal, and exists most likely due to the similar fate and transport characteristics of nitrate and Tc-99. In the oxidizing environment of the Hanford Formation, Tc-99 is in the valence state of Tc(VII) and forms pertechnetate (TcO_4^-). Ward et al. (2004) reports that the specific water chemistry of the antecedent water at the BCCT mixed with waste water may have created a condition of low sorptability for both anions. Cantrell et al. (2003) lists the partition coefficient of both TcO_4^- and NO_3^- as near zero.

Some ionic species contained in the waste do have significant sorptive capabilities, as shown with the phosphate concentration log in Figure 2. The phosphate ion is retarded relative to the nitrate, with much of its mass locked in the top 15m of the Hanford Formation. Although not shown, the U-238 (VI) correlates well with the phosphate, demonstrating that this pair may also have similar fate and transport characteristics to one another. The EC log shows a slight increase in the near surface that may correlate with the increased phosphate concentration. However, the influence of nitrate on the electrical properties of the pore-water is about 7 times that of phosphate. Correlations of EC from borehole C4191 with key analytes are shown in Table 1.

Table 1. Correlation coefficient among the various constituents in C4191 to EC

Species correlated to EC	Correlation coefficient	Max. Concentration (at depth in meters)
Tc-99 (VII)	0.89	$1.39x10^6$ pCi/L (30.8)
U-238 (VI)	-0.12	$2.5x10^4$ μCi/L (6.8)
Na^+	0.85	35,250 mg/L (27.7)
Ca^{+2}	0.85	6,230 mg/L (27.7)
K^+	0.62	710 mg/L (27.7)
Mg^{+2}	0.87	1,950 mg/L (27.7)
F^-	-0.24	90 mg/L (94.8)
Cl^-	0.86	760 mg/L (30.8)
NO_3^-	0.88	126,000 mg/L (30.8)
SO_4^{-2}	0.32	15,890 mg/L (24.7)
PO_4^{-3}	-0.15	750 mg/L (12.5)

A general characterization of electrical conductivity beneath the trench can be indicative of the nitrate concentration. Electrical conductivity, or its reciprocal, electrical resistivity, can be mapped from the surface using geophysics, which is an inexpensive characterization

methodology. Once the spatial distribution of nitrate is known, inferences can be made on the distribution of Tc-99, which traditionally has been mapped based on sampling of multiple boreholes.

Theory

Resistivity (ρ) is a volumetric property that describes the resistance of electrical current flow within a medium. Direct electrical current is propagated in rocks and minerals by electrolytic means. Electronic conduction only occurs in metallic-luster sulfide minerals, where free electrons are available. Rocks and non-metallic minerals have extremely high resistivities (low conductivities) and direct current transmission through this material is difficult. Porous media, on the other hand, carry current through ions by way of electrolytic conduction. Electrolytic conduction relies on the dissociated ionic species within a pore space. Here, the conduction varies with the mobility, concentration, and degree of dissociation. Electrolytic conduction is relatively slow with respect to electronic conduction due to mass transfer rate limiting processes and is strongly influenced by the structure of the medium.

Estimating resistivity is not a direct process. When current (I) is applied and voltage (V) measured, Ohms law is assumed and resistance is measured. Resistivity and resistance are then related through a geometric factor over which the measurement is made. The simplest example is a solid cylinder with a cross sectional area of A and length, L:

$$\rho = R\frac{A}{L} \qquad (1)$$

In such cases where the actual volume involved in the measurement is known, the result is called the "true" resistivity and is considered to be a physical property of that material. However, field measurements involve an unknown volume of earth. Consequently, resistivity calculations are based on the hypothetical response for the given electrode geometry over a homogeneous, isotropic, half-space. This results is what is termed "apparent" resistivity, but which is more accurately called a "half-space" resistivity.

Field data are generally acquired using an established electrode array. A four-electrode array employs electric current injected into the earth through one pair of electrodes (transmitting dipole) and the resultant voltage potential is measured by the other pair (receiving dipole). The ratio of the transmitted current and observed potential is called the transfer resistance. Some common electrode configurations are dipole-dipole, Wenner, and Schlumberger arrays. Their use depends upon site conditions and the information desired. Figure 3A, adapted from Telford et al. (1990), shows a schematic of the dipole-dipole configuration, where C1 and C2 are connected to the current source (i.e., transmitting electrodes) and P1 and P2 are connected to the volt-meter (receiving electrodes). For the four-electrode array, the geometric factor, K, is

$$K = 2\pi \frac{1}{\left(\frac{1}{r_1} - \frac{1}{r_2}\right) - \left(\frac{1}{r_3} - \frac{1}{r_4}\right)}, \qquad (2)$$

where r_1 through r_4 are defined in Figure 3A. Equations (1) and (2) are used to estimate an apparent resistivity, which assumes that each measurement of transfer resistance was a result of point electrodes on the surface of a homogeneous, isotropic, half-space:

$$\rho_a = 2\pi \frac{V}{I} K \qquad (3)$$

where subscript "a" in ρ_a denotes the *apparent* resistivity. The apparent resistivity is not necessarily the true resistivity of the formation, but a simplified resistivity that provides a starting point for subsurface evaluation. Other assumptions used in Equation 3 are isotropy (i.e., no directional dependence of resistivity), no displacement currents (using a DC or low frequency current application), and that resistivity is constant throughout such that Laplace's equation can be assumed. Since the degree of heterogeneity is not known *a priori*, a true resistivity is not calculated from Equation 3. To obtain a true resistivity, electrical resistivity tomography (ERT) is required, which generates a model of true resistivity using an iterative inverse methodology given the measurements of apparent resistivity, electrode arrangement, and other boundary conditions. Discussions of ERT and the methods by which the true resistivity is calculated can be found in several sources, including Loke and Barker (1996), LaBrecque et al. (1996), and Oldenburg and Li (1999).

Figure 3. Set up of the resistivity 4-pole array and pseudosection plotting methodology

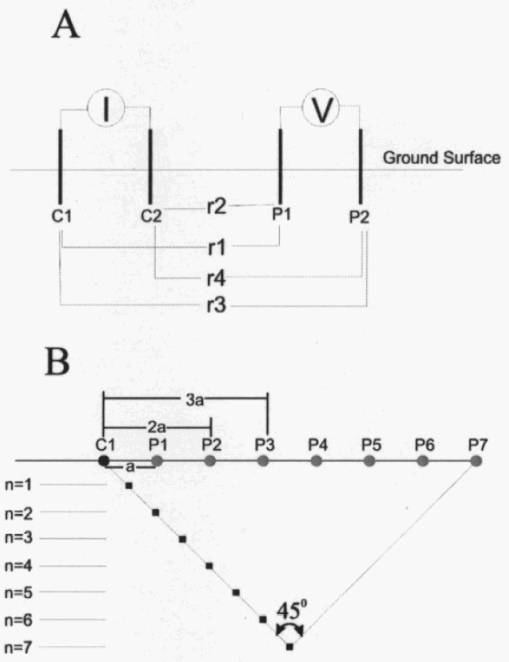

An alternative to the four-electrode array is the two-electrode pole-pole array. For the pole-pole array, one electrode from each of the current and potential pairs is fixed effectively at infinity, while the other current and potential electrodes act as "rover" electrodes within the survey transect. Practically, the infinite electrodes are spaced approximately 5 to 10 times the distance of the furthest separation of the rover electrodes, which can be up to 300 meters apart for a near

surface geophysical survey. The pole-pole array provides higher data density, increased signal to noise ratio, and requires less transmitted energy. Roy and Apparao (1971) discuss the superiority of the pole-pole method when conducting shallow surveys. Additionally, in some very conductive environments, where potential gradients are low, one may be forced to use the pole-pole array to simply measure a signal above the noise level of the data acquisition instrument.

The calculation of apparent resistivity is simplified in the pole-pole array:

$$\rho_a = 2\pi \frac{V}{I}(n * a) \tag{4}$$

where a is the basic electrode spacing and n is the integer multiplier as the current and potential electrodes incrementally separate. Figure 3B demonstrates a linear transect of electrodes on the surface with the a-spacing being the separation between each electrode and the n spacing increasing as the potential electrode moves away from the current electrode. The geophysical survey at the BCCT included a fixed a-spacing of 3 meters and n increased from 1 to 27. For a complete survey, each electrode has one turn at transmission, while potential measurements occur at all other electrodes in the array. Automated resistivity meters, such as the SuperSting R8 (Advanced Geosciences, Inc), has the ability to conduct multi-channel sweeps of potential measurements to significantly decrease measurement time.

Target Discrimination with Apparent Resistivity

The linear transect arrangement of electrodes produces a two-dimensional dataset of apparent resistivity as a function of x and z, where z is the dimension into the earth and x is along the surface. Although apparent resistivity is a function of the volume over which the measurement is made, its location is typically plotted as a point for ease of representation. The location of the point is a function of n and is loosely related to the depth of investigation. Hallof (1957) demonstrated that the intersection of two 45^0 lines extending downward from each of the current and voltage potential electrodes would produce a suitable pseudosection for interpretation. Others have used similar techniques to plot, for example, the depth to the maximum sensitivity in the electrode separation, (see Roy and Apparao, 1971). Using the Hallof approach, the pole-pole array has data plotted at a pseudo depth of:

$$-z_{pseudo} = 0.5na, \tag{5}$$

which is a linear plotting method.

Figure 4 is an apparent resistivity demonstration of several array types, including the pole-pole array, with a resistive half-space earth (400 ohm-m) and a graded conductive target (20 ohm-m). The target dimensions are 21x10m, and the top of the target is located at 10m below ground surface. The target was modeled with a forward resistivity model in EarthImager2D software (Advanced Geosciences, Inc. Austin, TX) using the basic algorithm of Dey and Morrison (1979). Many electrical resistivity modeling codes use some elements of this algorithm, including RES2DINV (Loke and Barker, 1996) and DCIP2D (Li and Oldenburg, 1994).

Qualitatively, the pole-pole apparent resistivity pseudosection in Figure 4 resembles the starting target more closely than the other arrays. The dipole-dipole and pole-dipole show extremely conductive "pantleg" effects, where the target's edge has been smeared diagonally downward. Since the apparent resistivity plotting routine contains information based on a volume-averaged measurement, artifacts such as pantlegs can be expected. The apparent resistivity plot of the Schlumberger array shows a straight vertical smearing as if it were a intrusive conductive dike. The pole-pole array, on the other hand, measures the electrical potential gradient relative to a fixed pole at infinity. In the earth, the infinite pole should essentially have no interaction with the electrical field and is modeled near the boundary condition of $V|_{\infty} = 0$. The result is a measurement of the actual potential as opposed to the gradient in potential measured for closely spaced dipoles, and a less pronounced pantleg smearing effect.

Figure 4. Apparent resistivity pseudosection comparisons for the Schlumberger, pole-dipole, dipole-dipole, and pole-pole array types for a discrete conductive target in a resistive homogeneous background

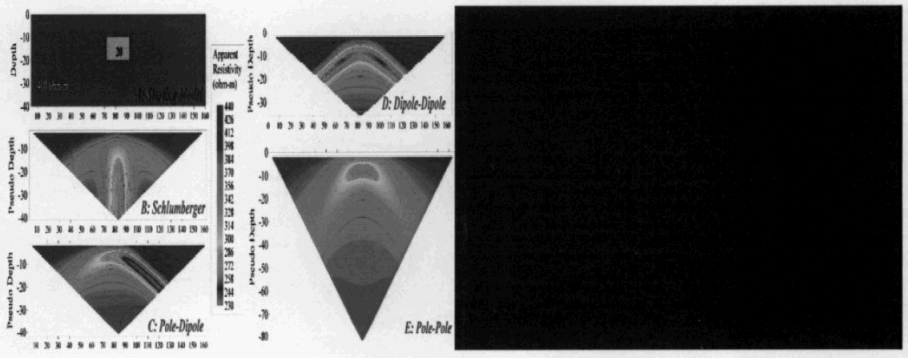

Another view of the apparent resistivity data can be seen in Figure 5, where vertical slices of data have been extracted at 81m (center of the domain) and at 65m. Figure 5A shows these slices as a function of the pseudo-depth for all but the pole-dipole array. In general, the pole-pole and dipole-dipole array show a decrease in resistivity at 81m (solid lines) that is loosely coincident with the target depth, while the Schlumberger array does not resemble the character of the target at all. Off-center at 65m (dashed lines), where the actual resistivity is a resistive homogeneous body, the pseudosection of the pole-pole shows less of an effect than the dipole-dipole. The Schlumberger array resembles the actual background better at the 65m slice.

Figure 5. A) Vertical slices through apparent resistivity data for Schlumberger, dipole-dipole, and pole-pole at 65m (beside target) and 81m (within target). B) Schematic of linear and nonlinear pseudosection plotting

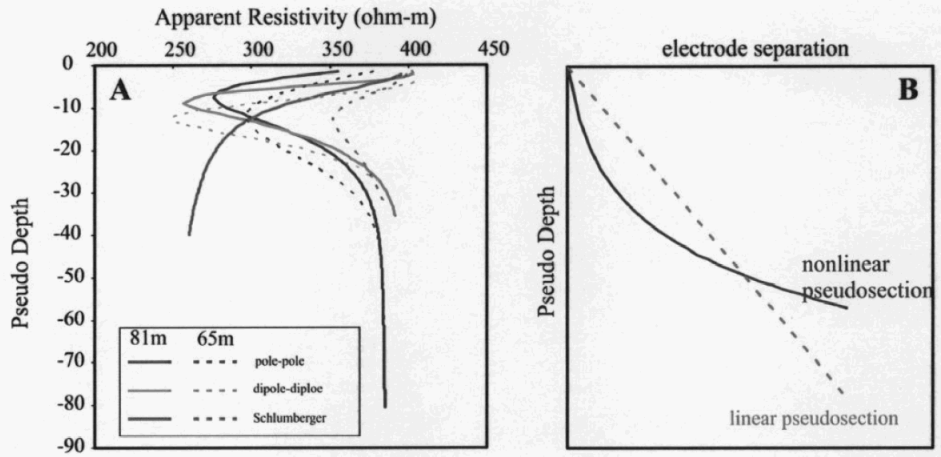

The depth of investigation stems from a need to relate a measurement made at the surface to some particular depth in order that survey parameters can be optimized for target identification (Barker, 1989). Before tomographic inversion was common practice among geophysicists to estimate the true resistivity from measured apparent resistivity, apparent resistivity pseudosections were used primarily for interpretation of subsurface electrical anomalies. Field practitioners became quite efficient at locating the depth to specific targets, such as ore bodies. The presentation of the pseudosection is important in these regards. Additionally, the pole-pole array, above all others, provides the weakest edge effects, thereby facilitating the direct interpretation of these data more reliably (Robain et al., 1999).

The traditional linear pseudosection of Hallof (1957) has limitations with respect to a physical meaning of the earth. Many researchers, therefore, have taken a closer examination of the plotting method to allow for a more reasonable geological interpretation. The most widely accepted depth of investigation studies are those presented by Roy and Apparao (1971), Roy (1972), and Koefoed (1972), who defined a depth of investigation characteristics (DIC) model for determining the depth of a measurement. The DIC was determined by finding the depth at which a thin horizontal layer within a homogeneous background makes the maximum contribution to the total measured signal at the surface. The results were consistent in that the depth of investigation is a nearly logarithmic function of electrode spacing, regardless of how the depth of investigation is defined. This suggests a modification of the linear pseudosection (Edwards, 1977; Fink 1980). Figure 5B shows an example of a nonlinear pseudosection, based on a logarithmically-based depth interpretation based on the electrode separation.

To facilitate the nonlinear depth plotting of apparent resistivity data, the logarithm of the n-spacing value was used in a 2nd-order polynomial:

$$-z_{\log} = u_1 \log(n)^2 + u_2 \log(n) + u_3 \qquad (6)$$

where z_{log} is the new interpreted depth location of the apparent resistivity value and $u_1 \ldots u_3$ are coefficients to be determined by using collocated target resistivity values. For this analysis, we are assuming that target data comes from a borehole, and therefore only the data from the vertical slice at 81m, i.e., same data from Figure 5A, will be used in finding coefficients $u_1 \ldots u_3$. The consequences of using an equation like Equation 6 are shown in Figure 5B, where the resistivity values near the surface are pushed deeper relative to the linear pseudosection and the deeper resistivity is pulled up relative to the linear pseudosection. At one point, the two plotting strategies have the same depth location for a given electrode separation.

The coefficients in Equation 6 can be determined using a nonlinear least-squares optimization procedure. To reduce the number of parameters, we equated u_1 and u_3 and the results of the transformation are shown in Figure 6A (with coefficients defined). Two other examples are shown in Figures 6B and 6C, where the target depth has moved down incrementally 10m. In each case, the parameters for the depth plotting of the nonlinear pseudosection have changed. Additionally, the minimum value of resistivity has increased as the target is placed deeper in the subsurface.

Figure 6. Vertical slices for comparison of interpretation of algorithms including pseudosection apparent resistivity and inverted true resistivity for a discrete conductive target at A) 10m below ground surface, B) 20m below ground surface, and C) 30m below ground surface.

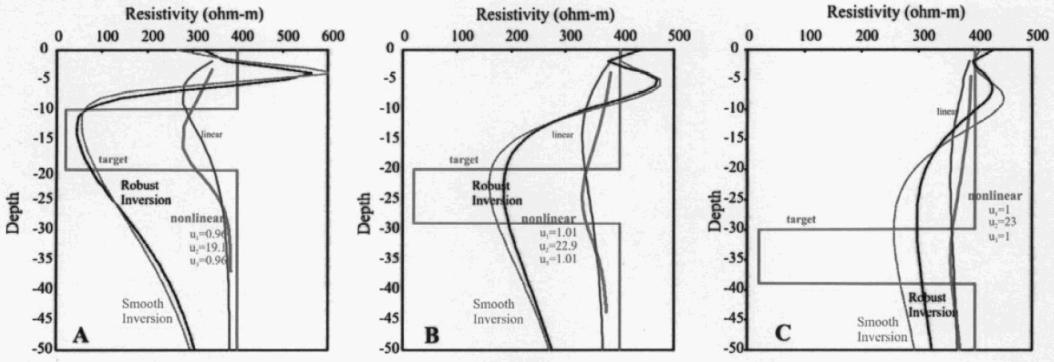

Typically after data collection, the apparent resistivity data are run through an inversion routine to estimate the true resistivity values that give rise to the measured resistivity. These models are based on either finite element or finite difference. In any case, the inversion method is nonlinear and requires an iterative solver. During the iterations, the distribution of true resistivities are estimated and the forward model calculates the voltage at the surface coincident with electrode locations. The differences between measured and modeled voltages are compared, and resistivities in regions showing large discrepancies are changed. The inversion model is run until the measured and modeled data are satisfactorily compared. In this way, the objective of the inversion is to minimize the difference between the modeled and measured resistivity, usually in a least squares sense. The objective function can be defined in many different ways, such as using the L_1-normalization (or robust inversion) or L_2-normalization (or smooth inversion) (Dahlin and Zhou, 2004). Compared to the damped least squares method with no normalization and L_1-normalization, the L_2-normalization is optimal at resolving smoother boundaries typical

for conductive plumes and most hydrologic boundaries (deGroot-Hedlin and Constable, 1990; de Groot-Hedlin and Constable, 2004; Loke et al., 2003).

Figure 7. Contours of resistivity for the different interpretation algorithms including linear pseudosection, nonlinear pseudosection, robust inversion (L_1-Normalization), and smooth inversion (L_2-Normalization).

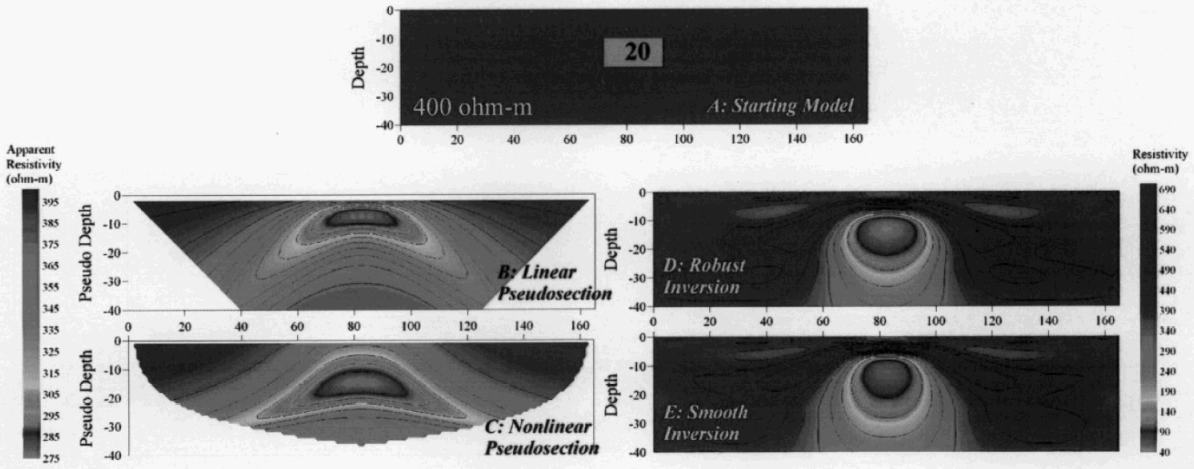

For the simple target problem identified in Figure 4, the measured apparent resistivity data were inverted using EarthImager2D. Both robust and smooth models were evaluated, with the results of the inversion shown in Figure 7. The final goodness-of-fit statistic, as measured by the root-mean-square error, was 0.91 and 0.67 for the robust and smooth inversion results, respectively. For comparison, the linear and nonlinear pseudosection data are plotted to the left of the inversion results. All of the contoured resistivity and apparent resistivity data show a target in the general location of the actual target location. Additionally, all methods appear to smear the information laterally or vertically, referring to a smooth condition where boundaries may not be as well defined. For the apparent resistivity plots, the lateral boundaries of the interpreted target are smeared by pantleg effects. For the inverted resistivity plots, the vertical information below the target is smeared.

To demonstrate the vertical smearing effects more concretely, Figure 6 includes vertical resistivity slices at 81m along the transect for both sets of inversions and for all three target models examined. In all three models, the minimum resistivity value is closer to the surface for the inversion results than the nonlinear pseudosection, but not as close as the linear pseudosection. Another major observation is that the gradient of resistivity is more asymmetrical for the inversion, where the change in resistivity to define the target is high close to the surface and low at depth. With these simplified models, it appears that the apparent resistivity may prove to be a useful tool for preliminary interpretation of simple discrete subsurface targets prior to inversion. Furthermore, if external information exists such as borehole information, the pseudo depth can be converted to a depth that is closer to the target horizon.

Figure 8. Geophysical survey map showing transect locations relative to the trenches

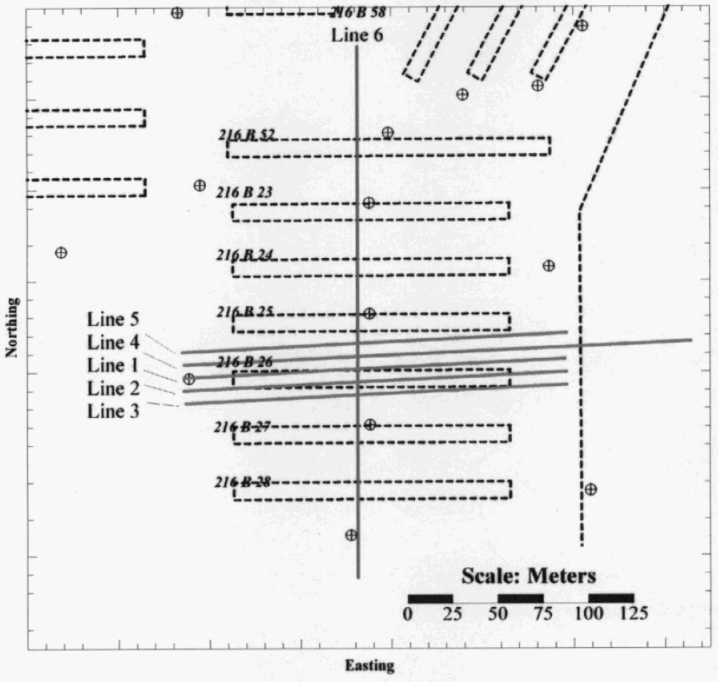

Geophysical Methodology and Results for Field Data

During the summer of 2004, a pilot geophysical electrical resistivity survey was conducted at the BCCT over trench 216-B-26. The survey included six two-dimensional lines, where five of the lines were run in the general direction of the trench and one was conducted perpendicular to the trench. Four of the five parallel lines were approximately 214m in length, with the fifth having a length of 316m. The offset between the parallel lines was 8m. The single line run perpendicular to the trench was located approximately midway along the parallel transects.

Figure 8 shows the geophysical survey layout at the BCCT. The electrical resistivity data were collected with the Sting R8 (Advanced Geosciences, Inc., Austin TX) using the SuperSting Smart electrode cables with 72 take-outs. The cables allow for easy roll-along operation to quickly collect data, with each roll-along consisting of 12 take-outs for the survey. The basic a-spacing was 2m for Lines 1-5 and 3m for Line 6.

Figure 9 shows the results of the apparent resistivity for the six transects, plotted with the nonlinear depth plotting algorithm. The depth locations of the nonlinear pseudosection were optimized based on the borehole data of electrical conductivity in Figure 2, with coefficients of **u**=[3.97, 22.4, 3.97]. The apparent resistivity data show that the low resistivity contours for transects 1-5 are primarily between the depths of 25-44m bgs. The low resistivity areas extend laterally out to the edges of the trench, where the electrical resistivity increases to approximately 400 ohm-m. For Line 6, which runs perpendicular over several trenches, the low resistivity contours are again located at the expected depth of high EC measured in borehole C4191. However, the low resistivity values extend from the surface beneath each of the trench locations

in a triangular shape. In particular, trench 216-B-52 appears to have a much larger low resistivity response, likely due to the fact that it received the most liquid waste of any trench, approximately 8500 m^3.

For completeness, the six resistivity lines were also inverted using EarthImager2D. The starting model for each line was the linear pseudosection. Other parameters include using the L_2-normalization (with a dampening and stabilization factor of 10.0), estimated error of 5% (for the covariance weighting matrix), and maximum and minimum resistivity of 10000 and 1 ohm-m, respectively. The goodness-of-fit as well as other statistics relevant to the study are shown in Table 2. The inverted resistivity lines of Figure 10 show a similar result as the logarithmic pseudosection of Figure 9, i.e., that a low resistivity plume exists beneath the site likely due to the disposal activities 50 years earlier. The inverted resistivity also shows the bottom edge of the plume to be less sharp than the borehole data suggest, which is a similar feature seen in the examples in Figure 7. Therefore, a truly Occam's approach to modeling this type of plume, where sharp gradients in the concentration profile exist, may be to simply work from the apparent resistivity plots for a qualitative interpretation of the target location, as opposed to inverting the data and getting back a blurred interpretation of the same plume.

Table 2. Resistivity Data and Inversion Statistics for BCCT

Statistic	Line 1	Line 2	Line 3	Line 4	Line 5	Line 6
data statistics						
Line Length (m)	214	214	214	314	214	321
# Electrodes	108	108	108	208	108	108
Elect. Separation (m)	2	2	2	2	2	3
Raw data count	5371	1372	1372	1909	1372	1372
Filtered data count*	4307	1273	1270	1800	1280	1289
Min ρ_a (ohm-m)	127	125	125	131	123	124
inversion statistics						
Inversion Iterations	3	2	2	3	3	3
Minimum Calc. ρ (ohm-m)	18.9	46.6	45.9	38.8	34.3	8.56
RMS (%)	3.81	3.50	4.56	3.46	3.53	3.23
L_2-Norm	0.58	0.49	0.83	0.48	0.50	0.42

*filtering data eliminates those measurements with high error, negative values, and data spikes

Since the electrical conductivity of the pore-water has been shown to be primarily a function of nitrate concentration, a scatter plot of the log-transformed nitrate concentration and resistivity data was constructed. Figure 11A shows the scatter plot for co-located apparent resistivity data obtained from Line 1 and nitrate with the linear least squares regression fit to the data. Again, for completeness, the inverted resistivity data are also presented in Figure 11B. From inspection,

Figure 9. Apparent resistivity plotted with nonlinear pseudosection collected over the waste sites at the BCCT Site.

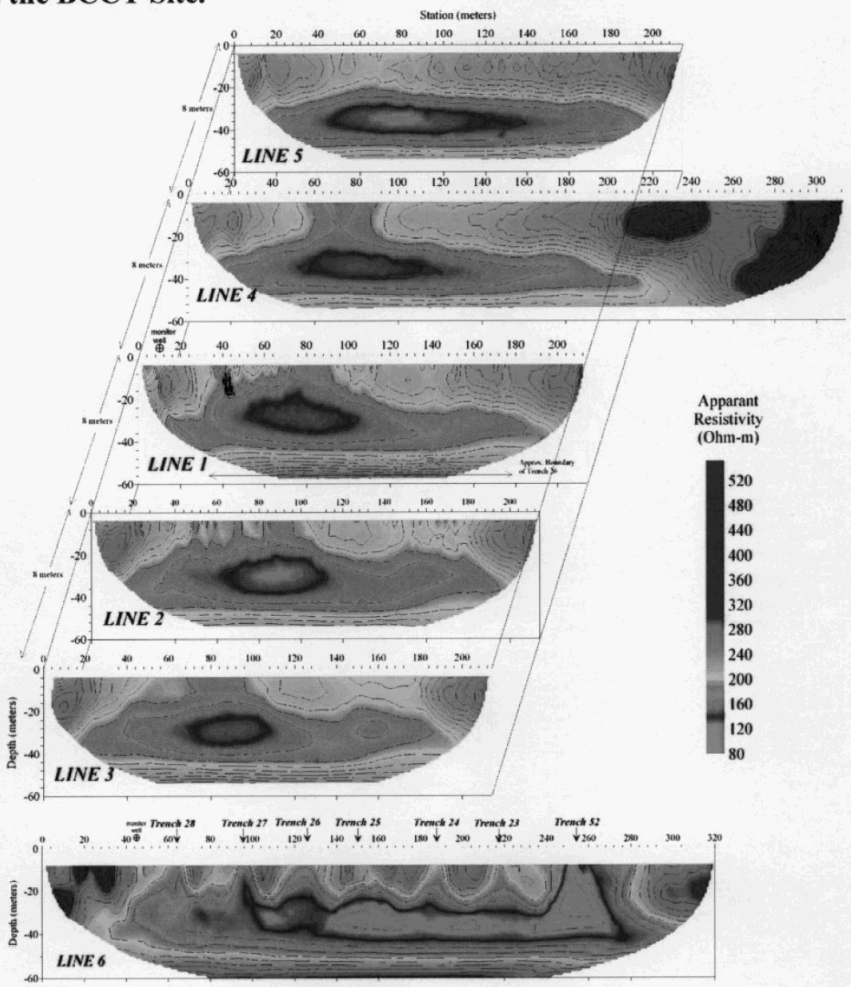

it appears that the inverted resistivity results should be segregated into two groups: regions above and below the nitrate plume that shows variability in the resistivity data, and within the plume. From this one borehole through the center of the waste site, where it is likely that the highest concentrations exist, the apparent resistivity plotting using a nonlinear depth algorithm, does a much better job at matching the plume's depth and height.

The correlation coefficient for the C4191-apparent resistivity data in Figure 11A is 0.951 and the nitrate concentration can be estimated from apparent resistivity data using the following transformation:

$$[NO_3^-] = 10^{a/\rho + b} \qquad (7)$$

where a and b are the slope and intercept for the regression data. The parameters for a and b are 505.2 and 1.207, respectively. The transformation equation and fitting parameters were used to convert the apparent resistivity data of Lines 1-5 to nitrate concentration in mg/L. The transformation revealed a minimum concentration of 187.2 mg/L and a maximum concentration

of 203,844 mg/L. The maximum concentration occurred in Line 5, 80m along the line at a depth of 31m bgs.

Figure 10. Inverted resistivity of the 6 lines presented in Figure 9 using smooth inversion.

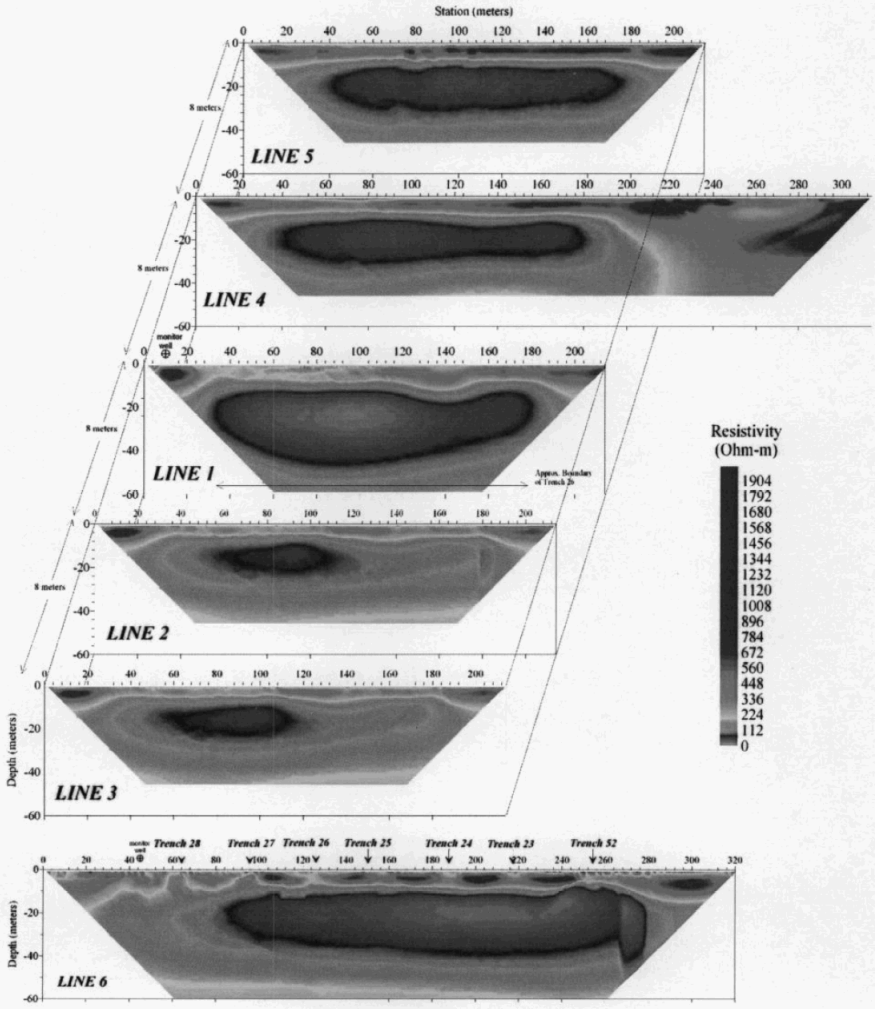

The three dimensional nitrate data set was rendered into a plume to show the spatial distribution of the data relative to the trenches. The rendering was possible due to the connectivity of the low resistivity values between transects, demonstrated in Line 6. An inverse distance interpolation algorithm was used to interpolate the data to a regularized grid with cell dimensions of 2m x 2m x 2m. Figure 12 shows the results of rendering, where two nitrate values were chosen to demonstrate the transformation. The smaller plume represents the larger concentration of 75,000 mg/L and the larger plume represents 35,000 mg/L. The figure also shows the relative locations of the trenches, wells, and resistivity transects, as well as the domain boundary of the rendered plume. Within this domain, the volume of soil that contains a nitrate concentration of 35,000 mg/L or more is 49,000 m^3 and the volume of soil containing 75,000 mg/L or more is 12,670 m^3. Outside the domain, no information is given and it is likely the low resistivity plume extends further north and south based on the positions of the other adjacent waste sites.

Figure 11. A) Apparent resistivity from Figure 9 versus nitrate concentration from borehole C4191 for co-located data along Line 1. B) Inverted resistivity from Figure 10 versus nitrate concentration.

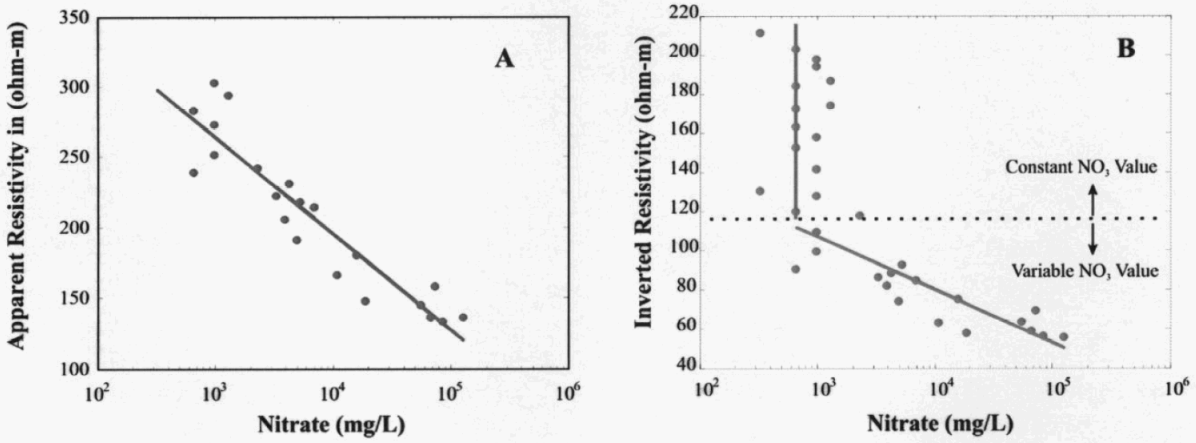

If water content values prior to disposal were known, the differences in water content could be potentially used to estimate the total mass of nitrate (M_{NO_3}) beneath the disposal site by:

$$M_{NO_3} = \sum_{\text{all cells}} (V_{\text{cell}} \cdot \Delta\theta) \cdot C_{NO_3} \qquad (8)$$

where the summation occurs over all cells, V_{cell} is the volume of the cell, C_{NO3} is the concentration of nitrate, and $\Delta\theta$ is the change in volumetric water content between the time prior to disposal and at the time of the resistivity measurement. The main assumption for the mass calculations, which is validated by the sorptivity data of nitrate, is that the nitrate resides primarily in the pore-water. The mass balance could be used to help confirm or refute the use of apparent resistivity in the direct conversion to concentration values. Alternatively, the inversion code could be accommodated to use the mass balance as a constraint.

Conclusions

A surface resistivity survey was conducted on the Hanford Site over a waste disposal trench that received a large volume of liquid inorganic waste. The objective of the survey was to map the extent of the plume that resulted from the disposal activities approximately 50 years earlier. A single confirmational borehole showed that the plume resided 25-44m below ground surface and that the electrical conductivity of the pore-water provided a potentially good target for surface geophysical measurements. The survey included five lines of resistivity of at least 200m in length and were oriented roughly parallel to the trench. A sixth line was placed perpendicular to the five parallel lines and ran over several adjacent trenches.

Figure 12. Three-dimensional rendering of the inferred nitrate plume beneath trench 216-B-26.

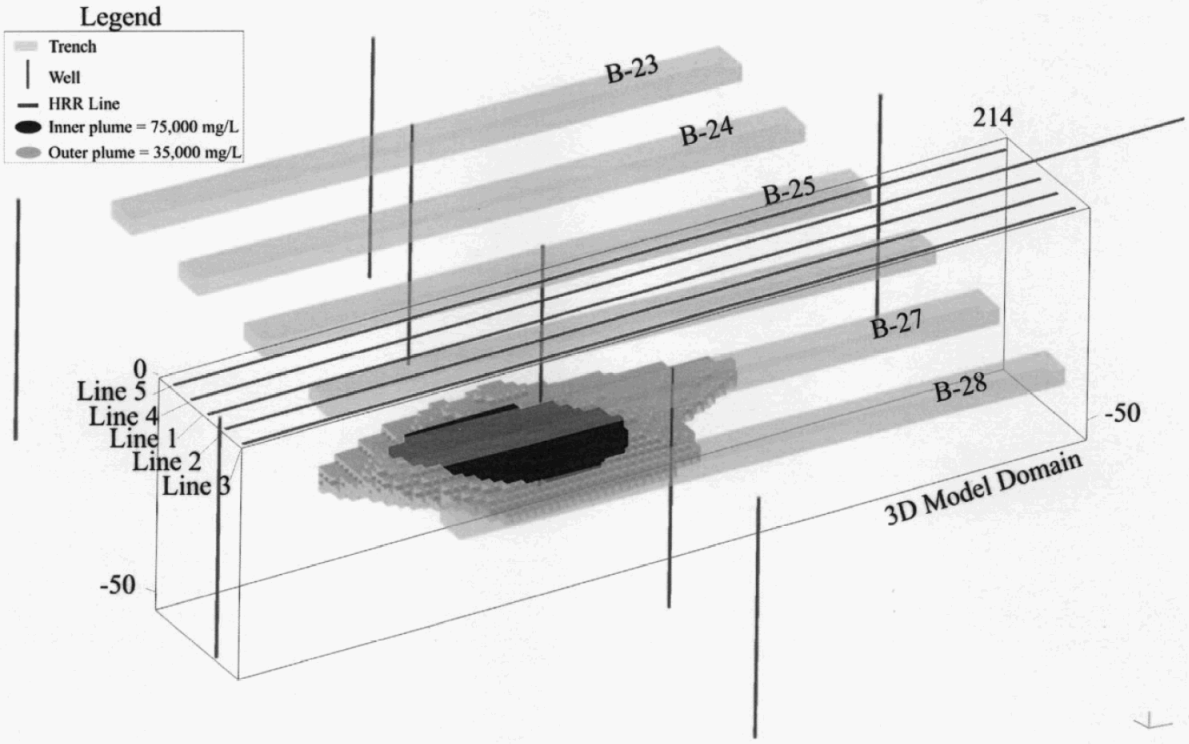

The pole-pole resistivity array was chosen based on its ability to collect a large sampling data set as well as having the ability to image deeper than the other arrays, such as the dipole-dipole or Wenner array. The resistivity data were presented as the apparent resistivity, which were calculated by an algorithm that assumes each measurement was collected within a homogeneous earth. This presentation style is referred to as a pseudosection, and is often the starting model for many electrical resistivity tomography (ERT) inversion algorithms. The advantage of the apparent resistivity pseudosection is that it displays actual measured data as opposed to an interpretation of the data obtained with ERT. Furthermore, the pseudosection of the pole-pole array provides the weakest edge effects, thereby facilitating the direct interpretation of resistivity data more reliably (Robain et al., 1999).

The disadvantage of the pseudosection interpretation methodology is that the depth location of the resistivity data point often lacks physical meaning. Hallof (1957) showed that a linear plotting algorithm was sufficient for the interpretation. Others have shown that the pseudosection can be more meaningful by calculating the depth of maximum sensitivity. Within our analysis, we show that the pseudosection can be plotted meaningfully if direct sampling information is incorporated into the target depth estimation. For the BCCT, a logarithmic function was used and the fitting parameters for estimating depth were obtained through a least squares methodology using the known borehole data. The results of this plotting methodology indicated that a low resistivity plume resides directly beneath all of the waste trenches that were

imaged, but the edges of the plume are likely contained within the outer bounds of the footprint defining the trenches.

The relations developed to show the electrical conductivity (EC) highly correlated to nitrate and the apparent resistivity highly (and indirectly) correlated to EC provide a mechanism by which an inference can be made to correlate resistivity to nitrate. This correlation was used to develop a transformation function to convert the resistivity to nitrate and render a three dimensional depiction of the nitrate plume directly beneath trench 216-B-26. The major assumptions used for the transformation was that the resistivity anomaly is primarily caused by nitrate and that the nitrate data from the borehole sample is representative within the measurement area. One could take the step to estimate, using the same procedure, the spatial distribution of Tc-99, given the same high correlations to EC. Lastly, if resistivity measurements could be conducted over the entire BCCT site, perhaps the fate of the nitrate could be better understood and risk minimized to populations downgradient of the site. To accurately map the entirety of the BCCT, however, it is recommended that more borehole samples be gathered to ensure high correlations to the analyte of interest.

Acknowledgements
Special thanks go to Mark Benecke of Fluor Hanford, Inc. and Mark Sweeney of Pacific Northwest National Laboratory. The work was performed for Fluor Hanford Group and the U.S. Department of Energy under Contract DE-AC05-76RL01830.

References

Abu-Zeid, N., G. Bianchini, G. Santarato, and C. Vaccaro, 2003. Geochemical characterisation and geophysical mapping of Landfill leachates: the Marozzo canal case study (NE Italy). Environmental Geology (2004) 45:439–447.

Adepelumi, A.A., B. D. Ako, O. Afolabi, and J. B. Arubayi, 2005. Delineation of contamination plume around oxidation sewage-ponds in Southwestern Nigeria. Environmental Geology 48(8): 1137-1146.

Barker, R.D., 1989. Depth of investigation of collinear symmetrical four-electrode arrays. Geophysics 54(8):1031-1037.

Brodeur, J.R., R.K. Price, R.D. Wilson, C.J. Koizumi, 1993. Results of Spectral Gamma-Ray Logging of Select Boreholes for the Aggregate Area Management Study. WHC-SD-EN-TI-021, Westinghouse Hanford Company, Richland, WA.

Cantrell, K.J., R.J. Serne, and G. V. Last, 2003. Hanford Contaminant Distribution Coefficient Database and Users Guide. PNNL-13895. Pacific Northwest National Laboratory, Richland, WA.

Chambers, J.E., O. Kuras, P.I. Meldrum, R.D. Ogilvy, and J. Hollands, 2006. Electrical resistivity tomography applied to geologic, hydrogeologic, and engineering investigations at a former waste-disposal site. Geophysics 71(6): B231–B239.

Connelly, M.P., B.H. Ford, and J.V. Borghese, 1992. Hydrogeologic Model for the 200 West Groundwater Aggregate Area. WHC-SD-EN-TI-014, Rev 0, Westinghouse Hanford Company, Richland, WA.

Corbin, R.A., B.C. Simpson, M.J. Anderson, W.F. Danielson III, J.G. Field, T.E. Jones, and C.T. Kincaid, 2005. Hanford Soil Inventory Model, Rev. 1. PNNL-15367, Pacific Northwest National Laboratory, Richland, WA.

Dahlin, T. and B. Zhou, 2004. A numerical comparison of 2D resistivity imaging with 10 electrode arrays. Geophysical Prospecting, 52:379–398.

deGroot-Hedlin, C. and Constable, S., 1990. Occam's inversion to generate smooth, two-dimensional models from magnetotelluric data. Geophysics, 55(12): 1613-1624.

de Groot-Hedlin, C. and Constable, S., 2004. Inversion of magnetotelluric data for 2D structure with sharp resistivity contrasts. Geophysics, 69(1): 78-86.

Dey, A. and H.F. Morrison, 1979. Resistivity modeling for arbitrarily shaped three-dimensional structures. Geophysics 44(4): 753-780.

Edwards, L. S., 1977. A Modified Pseudosection for Resistivity and IP. Geophysics 43(5): 1020-1036.

Fecht, K.R., G.V. Last, and K.R. Price, 1977. Evaluation of Scintillation Probe Profiles from 200 Area Crib Monitoring Wells, ARH-ST-156, Atlantic Richfield Hanford Company, Richland, WA.

Fink, J.B., 1980. Logarithmic Pseudosections. Abstract, Proceedings of the 50th Ann. Mtg. Soc. Expl. Geophysicists.

Gephart, R.E. and R.E. Lundgren, 1998. Hanford Tank Cleanup: A Guide to Understanding the Technical Issues. Battelle Press. Richland, WA.

Griffin, R.A. and J.J. Jurinak, 1973. Estimation of activity coefficients from the electrical conductivity of natural aquatic systems and soil extracts. Soil Science 116:26-30.

Hallof, P.G., 1957. On the interpretation of resistivity and induced polarization measurements. PhD Dissertation, MIT.

Horton, D.G. and R.R. Randall, 2000. Results of the 1999 Spectral Gamma-Ray and Neutron Moisture Monitoring of Boreholes at Specific Retention Facilities in the 200 East Area, Hanford Site. PNNL-13077, Pacific Northwest National Laboratory, Richland, WA.

Kincaid, C. T., P. W. Eslinger, R. L. Aaberg, T. B. Miley, I. C. Nelson, D. L. Strenge, and J. C. Evans, Jr. , 2006. Inventory Data Package for Hanford Assessments. PNNL-15829, Pacific Northwest National Laboratory, Richland, WA.

Koefoed, O., 1972. Discussion on "Depth of investigation in direct current methods." By A. Roy and A. Apparao. Geophysics 37(5):703-704.

LaBrecque, D.J., M. Miletto, W. Daily, A. Ramirez, and E. Owen, 1996. The effects of noise on Occam's inversion of resistivity tomography data. *Geophysics*, 61(2):538-548.

Li, Y. and D.W. Oldenburg, 1994. Inversion of 3-D DC resistivity data using an approximate inverse mapping. Geophysical Journal International, 116:527-537.

Loke, M.H. and R.D. Barker, 1996. Rapid least-squares inversion of apparent resistivity pseudosections by a quasi-Newton method. Geophysical Prospecting 44(1):131–152.

Loke, M.H., Acworth, I. and Dahlin, T., 2003. A comparison of smooth and blocky inversion methods in 2D electrical imaging surveys. Exploration Geophysics, 34(3): 182-187.

Marion, G.M. and K.L. Babcock, 1976. Predicting specific conductance and salt concentration in dilute aqueous solutions. Soil Science 122:181-187.

O'Farrell, T. P., and R. O. Gilbert. 1975. Transport of radioactive materials by jackrabbits on the Hanford Reservation. Health Physics 29:9–15.

Oldenburg, D.W. and Y. Li, 1999. Estimating depth of investigation in DC resistivity and IP surveys. Geophysics 64(2):403-416.

Paine, J.G., 2003. Determining salinization extent, identifying salinity sources, and estimating chloride mass using surface, borehole, and airborne electromagnetic induction methods. Water Resources Research, Vol. 39, No. 3, 1059, Doi:10.1029/2001wr000710.

Robain, H., Y. Albouy, M. Dabas, M. Descloitres, C. Camerlynck, P. Mechler, Pierre and A. Tabbagh, 1999. The location of infinite electrodes in pole-pole electrical surveys: Consequences for 2D imaging. Journal of Applied Geophysics, 41(4):313-333.

Roy, A., 1972. Depth of investigation in Wenner, three-electrode, and dipole-dipole DC resistivity methods. Geophysical Prospecting 20:329-340.

Roy, A. and A. Apparao, 1971. Depth of investigation in direct current methods. Geophysics 36(5):943-959.

Rucker, D.F. and M.D. Sweeney, 2004. Plume delineation in the BC Cribs and Trenches Area, PNNL-14498. Pacific Northwest National Laboratory, Richland, WA.

Serne, R. J., et al., 2002. Characterization of Vadose Zone Sediment: Borehole 41-09-39 in the S-SX Waste Management Area, PNNL-13757-3, Pacific Northwest National Laboratory, Richland, WA.

Serne, R.J and F.M. Mann 2004. Preliminary Data from 216-B-26 Borehole in BC Cribs Area. RPP-20303, Rev. 0. CH2MHill Group, Richland, WA.

Telford, W.M., L.P. Geldart, and R.E. Sheriff, 1990. Applied Geophysics. Cambridge University Press, Cambridge, UK.

Titov, K.V., A. Levitski, P.K. Konosavski, A.V. Tarasov, Y.T. Ilyin, and M.A. Bu`es, 2005. Combined application of surface geoelectrical methods for groundwater-flow modeling: A case history. Geophysics 70(5): H21-H31.

U.S. DOE, 2003. BC Cribs and Trenches 200-TW-1 Operable Unit Borehole Sampling and Analysis Plan. DOE/RL-2003-44, Rev 0-2003. U.S. Department of Energy, Richland Operations Office, Richland, WA.

Ward, A.L., G.W. Gee, Z.F. Zhang, J.M. Keller, 2004. Vadose Zone Contaminant Fate-and-Transport Analysis for the 216-B-26 Trench. PNNL-14907. Pacific Northwest National Laboratory, Richland, WA.

Watson, D.B., W.E. Doll, T.J. Gamey, J.R. Sheehan, and P.M. Jardine, 2005. Plume and lithologic profiling with surface resistivity and seismic tomography. Ground Water 43(2):169-177.